Activated hepatic stellate cells with senescence-associated secretory phenotype signature in steatohepatitic hepatocellular carcinoma

Jee San Lee

Department of Medical Science

The Graduate School, Yonsei University

Activated hepatic stellate cells with senescence-associated secretory phenotype signature in steatohepatitic hepatocellular carcinoma

Directed by Professor Young Nyun Park

The Master's Thesis
submitted to the Department of Medical Science,
the Graduate School of Yonsei University
in partial fulfillment of the requirements for the degree of
Master of Medical Science

Jee San Lee

December 2014

This certifies that the Master's Thesis of
Jee San Lee is approved.

Thesis Supervisor: Young Nyun Park

Thesis Committee Member#1: Jin Sub Choi

Thesis Committee Member#2: Haeryoung Kim

The Graduate School
Yonsei University

December 2014

ACKNOWLEGEMENTS

먼저, 이 논문이 완성되기 까지 많이 부족했던 저에게 아낌없는 지도, 격려, 인내 그리고 배려를 해주신 박영년 교수님께 깊은 감사드립니다. 그리고 제 논문을 지도해 주시고 많은 조언을 해주신 최진섭 교수님, 김혜령 교수님께 감사의 말씀 드립니다.

또한, 이 논문이 완성되기 까지 너무나 많은 도움을 주신 병리학교실 분들께 감사의 말씀 드립니다. 면역염색 및 면역형광 염색을 잘 세팅할수 있도록 도와주고 항상 격려해 주신 유정은 선생님, 환자 데이터 및 분석에 많은 도움을 주시고 다방면으로 도와주셨던 이형진 선생님, 이 논문의 큰 틀을 잡아주신 고명주 선생님, 면역 염색 분석 및 병리 분석 방법을 차근차근 알려주신 남지해 선생님, 슬라이드를 깎아주시고 항상 진심 어린 조언을 주셨던 방근배 선생님, 블록을 찾아주신 차종훈 선생님, 염색 방법 및 실험 방법에 많은 조언을 주신 오성근, 박원영 선생님, 많은 격려를 해주신 김영주 선생님, 그리고 언니이자 동기이고 친구 같은 나의 모든걸 이해해준 그리고 나에게 정말 아낌없었던 고정은 선생님, 모두에게 너무나 많은 감사드립니다. 선생님들의 도움이 없었으면 이 논문은 없었을 것입니다. 그리고 마지막으로 항상 옆에서 나를 응원해 주었던 친구들에게 너무 고맙고 끝없이 응원을 해준 우리 가족과 친척분들께 감사의 말씀을 전하고 싶습니다.

이지산

<TABLE OF CONTENTS>

LIST OF FIGURES

LIST OF TABLES

<ABSTRACT>

Activated hepatic stellate cells with senescence-associated secretory phenotype signature in steatohepatitic hepatocellular carcinoma

Jee San Lee

Department of Medical Science

The Graduate School, Yonsei University

(Directed by Professor Young Nyun Park)

Steatohepatitic hepatocellular carcinoma (HCC), a new histologic variant of HCC has been recently reported in patients with metabolic syndrome or hepatitis C virus–related cirrhosis with associated non-alcoholic fatty liver disease (NAFLD). The incidence of metabolic syndrome has rapidly increased in Asia including Korea, where hepatitis B virus (HBV) is the main etiology of HCC. However, clinicopathological features of steatohepatitic HCC in HBV patients with metabolic syndrome and its molecular pathogenesis remain unclear. Steatohepatitic HCCs (n = 21) and conventional HCCs (n = 34) were selected from non-C viral, non-alcoholic and non-autoimmune hepatitis patients, and the HBV infection was evaluated by serological test of HBsAg or HBV DNA nested PCR using liver tissue. Their difference in clinical, and molecular pathological aspects was analyzed focusing hepatic stellate cell activation and senescence-associated secretory phenotype (SASP). The expression of α-smooth muscle actin (α-SMA), $p21^{Waf1/Cif1}$, γ-H2AX,

IL-6, and Ki-67 were investigated by single or double immunohistochemistry or immunofluorescence. Steatohepatitic HCCs showed significantly older age, higher body mass index, higher incidence of diabetes, central obesity, hypertriglyceridemia and NAFLD compared to conventional HCCs (P <0.05 for all). Metabolic syndrome was more prevalent in steatohepatitic HCCs compared to conventional HCCs (P= *0.*029), whereas the incidence of HBV infection showed no significant difference between two groups. Activated hepatic stellate cells expressing $p21^{Waf1/Cif1}$, IL-6 (P <0.05 for both) and γ-H2AX (P = 0.066) were more frequently found in steatohepatitic HCCs compared to conventional HCCs. Non-tumoral liver of steatohepatitic HCCs also showed higher number of activated stellate cells expressing γ-H2AX and $p21^{Waf1/Cif1}$ compared to that of conventional HCCs (P <0.05 for both). There was no significant difference of Ki-67 expressing activated hepatic stellate cells between steatohepatitic and conventional HCCs in both of tumoral and non-tumoral lesions.

Therefore, steatohepatitic HCC is suggested as a distinctive variant of HCC in metabolic syndrome with or without chronic B viral hepatitis. Activated hepatic stellate cells expressing senescence-associated protein ($p21^{Waf1/Cif1}$ and γ-H2AX) and SASP factor (IL-6) are considered to be important in the pathogenesis of steatohepatitic HCC.

Key Words: hepatocellular carcinoma, steatohepatitic hepatocellular carcinoma, non-alcoholic fatty liver disease, metabolic syndrome, activated hepatic stellate cells, senescence-associated secretory phenotype

Activated hepatic stellate cells with senescence-associated secretory phenotype signature in steatohepatitic hepatocellular carcinoma

Jee San Lee

Department of Medical Science

The Graduate School, Yonsei University

(Directed by Professor Young Nyun Park)

I. INTRODUCTION

Non-alcoholic fatty liver disease (NAFLD) encompasses a spectrum of fatty liver diseases, ranging from simple steatosis, to non-alcoholic steatohepatitis, fibrosis, and ultimately cirrhosis[1,2]. The incidence of hepatocellular carcinoma (HCC) is increasing gradually in association with metabolic syndrome[3, 4].The prevalence of metabolic syndrome is increasing in Asia including in Korea[5]. Obesity together with diabetes, also increase the risk of HCC development to approximately 100 fold in patients with hepatitis C virus (HCV) and hepatitis B virus (HBV)[6].

Recently, a histologically distinct subtype of HCC showing features of steatohepatitis within the tumor region has been pathologically characterized and introduced as a new category, termed steatohepatitic HCC[7]. This newly defined HCC variant histologically resembles non-neoplastic steatohepatitis, characterized by large droplet steatosis in tumor cells, pericellular fibrosis, inflammation,

ballooning, and Mallory-Denk body formation. In addition, steatohepatitic HCC variant is associated with metabolic syndrome[7-9]. Most studies about steatohepatitic HCC have mainly dealt with HCC patients with HCV, and the clinicopathological features of steatohepatitic HCC in HBV patients - which is the main etiology of HCC in Asia including Korea - remains unclear[10].

The activation of hepatic stellate cells in chronic liver disease including NAFLD has been demonstrated in association with several conditions, including fatty change, reactive oxygen species generation and DNA damage etc[11]. In response to these stimuli, hepatic stellate cells undergo phenotypic conversion from quiescent retinoid-storing cells to active myofibroblastic cells and ultimately affect fibrosis progression[12]. Interestingly, dietary or genetically-induced obesity in mice led to alterations in intestinal microbiomes and deoxycholic acid (DCA) production, which in turn induced senescence-associated secretory phenotype (SASP) in hepatic stellate cells and promoted obesity-associated HCC development[13]. This study demonstrated that senescence-associated markers such as p21, p16 and γ-H2AX were up-regulated in the tumor region, particularly in the activated hepatic stellate cells and these cells produced SASP factors[13]. In steatohepatitic HCCs increased number of activated hepatic stellate cells were observed, however its relation with SASP factors have not been demonstrated[8]. In the present study, clinicopathological features of steatohepatitic HCC in metabolic syndrome with HBV and its molecular pathogenesis was investigated focusing on the hepatic stellate cell activation and senescence associated protein and SASP factor including $p21^{Waf1/Cif1}$,γ-H2AX, Ki-67 and IL-6.

II. MATERIALS AND METHODS

1. Case selection and histopathological examination

We reviewed the pathological and clinical records of consecutive HCC patients who underwent partial hepatectomy or liver transplantation between 2009 and 2014, from the archives of the Department of Pathology, Yonsei University College of Medicine. Patients who underwent chemotherapy or locoregional therapy (such as transarterial chemoembolization or radioactive frequency ablation) before surgery were excluded from this study. We excluded patients with histories of excessive alcohol consumption (defined as >40 g/day), viral hepatitis C, D and E, and autoimmune disease. The status of hepatitis B virus surface antigen (HBsAg) was reviewed. Formalin-fixed, paraffin-embedded tissue sections stained with hematoxylin-eosin (H&E) and Masson's trichrome were reviewed for all cases. When multiple tumors were present, the largest tumor was selected for assessment. The histopathologic characteristics of each HCC was assessed and recorded, especially focusing on features of steatohepatitis as follows[8]; 1) large-droplet fat within the tumor: absent/minimal (0% to 4%), mild (5% to 33%), moderate (34% to 60%) and severe (>60%); 2) ballooning change: none, focal, marked ; 3) Mallory-Denk bodies: absent, present ; 4) pericellular fibrosis: thin strands of fibrosis with a "chicken-wire" appearance: none, focal, marked ; 5) inflammation, including neutrophils and lymphocytes: minimal (<2 foci of inflammatory cells under the 10x objective), mild (2 to 5 foci of inflammatory cells under the 10x objective), and moderate (>5 foci of inflammatory cells under the 10x objective). Steatohepatitic HCCs was selected based on the following criteria: a combination of at least four of the above features in ≥50% of the tumor area. For comparison, conventional HCCs which have typical histopathological features of HCCs were selected. For normal

control liver, 5 non-neoplastic liver samples from liver donors or non-neoplastic livers adjacent to metastatic carcinomas were used. The control samples were negative for HBV and showed relatively normal liver histology.

Other histopathological features of each case, including size, capsule formation, major and worst grades of differentiation, and presence of vascular invasion were also noted. The non-tumor liver was assessed and scored for steatosis and evidence of steatohepatitis. The degree of steatosis in the parenchyma was classified as absent/minimal (0% to 5%), mild (6% to 30%), moderate (31% to 60%), and severe (>60%) [14]. In addition, according to the US National Cholesterol Education Program Adult Treatment Panel III (NCEP ATP III, 2001) and International Diabetes Federation (IDF) ethnicity waist circumference criteria, we reviewed the clinical charts for the presence of metabolic syndrome risk factors: central obesity [waist circumference >90 cm in men and >80 cm in women and body mass index (BMI)], hypertriglyceridemia [serum triglycerides (≥150 mmHg) or current use of antidyslipidemia medication], low high-density lipoprotein cholesterol [(<40 mg/dL) in men and (<50 mg/dL) in women], diabetes [elevated fasting plasma glucose levels (≥100 mg/dL) or current use of anti-diabetic medication] and hypertension [systolic blood pressure (≥130 mmHg) or diastolic blood pressure (≥85 mmHg) or current use of blood pressure medication][15, 16].

2. Immunohistochemistry and immunofluorescence

Formalin-fixed paraffin-embedded tissues were cut into 4μm-thick sections. The paraffin embedded sections were deparaffinized for an hour and rehydrated in graded alcohol and in distilled water for 1 minute each at room temperature. For immunohistochemistry, sections were soaked in 3% H_20_2 for 15 minutes to block the endogenous peroxidase. After washing, antigen retrieval was performed. A complete list of the primary antibodies used and the antigen retrieval conditions are described in Table 1. The primary antibody IL-6 was applied to the slide and incubated for an hour at room temperature. After rinsing, incubation with a secondary antibody was performed for 20 minutes using DAKO Envision kit (Dako, Glostrup, Denmark), and visualized with 3,3-diaminobenzidine (DAB). Sections were counterstained with Mayer's hematoxylin for 7 minutes and rinsed in tap water for 20 minutes. Slides were then dehydrated and mounted. For the double immunohistochemistry [alpha-smooth muscle actin (α-SMA) and $p21^{Waf1/Cip1}$], $p21^{Waf1/Cip1}$ primary antibody was applied to the slides, left overnight in 4 ℃, and then treated with Vector Blue Alkaline Phosphatase Substrate Kit III (SK-5300; Vector Laboratories, Burlingame, CA, USA). Next, α-SMA (Dako, Glostrup, Denmark) primary antibody was applied for an hour at room temperature. Secondary antibody was applied using the DAKO Envision kit, and then developed with DAB. Double immunofluorescence was carried out to assess the phosphorylation of histone H2AX at ser139 (γ-H2AX) and the expression levels of Ki-67 and IL-6 in activated hepatic stellate cells. After deparaffinization and rehydration as described above, sections were soaked twice in 1%$NaHB_4$ for 5 minutes each to block the endogenous peroxidase. Before staining for γ-H2AX/α-SMA (Dako, Glostrup, Denmark) and Ki-67/α-SMA (Abcam, Cambridge, MA,

USA) sections were pretreated in 10mM citrate buffer (pH6.0) in a microwave for 20min for antigen retrieval. Blocking step was followed for 30 minutes using 5%BSA, and two primary antibodies raised in different species [γ-H2AX/α-SMA (Dako, Glostrup, Denmark), IL-6/α-SMA (Dako, Glostrup, Denmark) and Ki-67/α-SMA (Abcam, Cambridge, MA, USA)] were applied to the slides. After rinsing the primary antibody, Alexa fluor 594 (red) goat anti rabbit IgG and Alexa fluor 488 (green) donkey mouse IgG conjugated antibodies (Invitrogen, Carlsbad, CA, USA) were applied for 60 minutes. The slides were washed in the dark and nuclei were stained with 4'-6' diamidino-2-phenylindole (Life Technologies, Gaithersburg, MD, USA) and left to dry for 2 days in the dark before imaging in the microscope. For ubiquitin, an XT automated stainer (Ventana, Tucson, AZ, USA) was used.

Table 1. List of antibodies used for the immunohistochemistry and immunofluorescence

Antibody	Source	Dilution	Antigen retrieval
α-SMA (mouse mAb; clone 1A4)	Dako (Glostrup, Denmark)	1:1000	Microwave, citrate (pH 6.0) or no treatment
α-SMA (rabbit pAb)	Abcam (Cambridge, MA, USA)	1:300	Microwave, citrate (pH 6.0)
$p21^{Waf1/Cip1}$ (rabbit mAb; 12D1)	Cell signaling (Danvers, MA, USA)	1:50	Microwave, citrate (pH 6.0)
γ-H2AX (rabbit mAb; 20E3)	Cell signaling (Danvers, MA, USA)	1:150	Microwave, citrate (pH 6.0)
IL-6 (rabbit pAb)	Abcam (Cambridge, MA, USA)	1:100	Protease K or no treatment
Ki-67 (mouse mAb; MIB-1)	Dako (Glostrup, Denmark)	1:100	Microwave, citrate (pH 6.0)
Ubiquitin (rabbit pAb)	Dako (Glostrup, Denmark)	1:200	Microwave, citrate (pH 6.0)

Abbreviations: α-SMA, α-smooth muscle actin; mAb, monoclonal antibody; pAb, polyclonal antibody
* No treatment for immunofluorescence

3. Interpretation of staining results

The immunohistochemical stain results for IL-6 and $p21^{Waf1/Cip1}$ (nuclear staining in tumoral and non-tumoral hepatocytes) was assessed. The staining intensity was graded on a scale of 0~3 (0, negative; 1, weakly positive; 2, moderately positive; and 3, strongly positive), and the extent of distribution was rated on a scale of 0~4 (0, positive in <5% of cells; 1, 5~25%; 2, 26~50%; 3, 51~75%; and 4, 76~100%). The histoscore was defined as the sum of the intensity and distribution scores. Positive staining was defined as staining scores of 4~7 whereas 0~3 were regarded as negative. To assess the number of activated hepatic stellate cells, 20 photomicrographs were taken at original magnification x400 then the α-SMA positive cells were counted for each picture. α-SMA expressed in the blood vessels or bile ducts were excluded. For the $p21^{Waf1/Cip1}$/α-SMA co-stained cells, the number of α-SMA positive cells and $p21^{Waf1/Cip1}$/α-SMA co-stained cells were counted in 20 randomly selected fields (original magnification x400). The average number for $p21^{Waf1/Cip1}$/α-SMA co-stained cells were calculated by dividing total number of $p21^{Waf1/Cip1}$/α-SMA co-stained cells by the total number of α-SMA positive cells and multiplied by 100%. For the γ-H2AX/α-SMA, IL-6/α-SMA and Ki-67/α-SMA co-stained cells, at least 100 α-SMA positive cells were counted at original magnification x200 and the average number of co-stained cells was calculated as described above. The presence or absence of Mallory-Denk bodies were evaluated by immunoreactivity for ubiquitin. For the interpretation of the γ-H2AX and Ki-67 labeling indices (LI) (nuclear staining in tumoral and non-tumoral hepatocytes), more than 1000 cells were counted in random areas of the tissue section and was calculated as the percentage of positively stained nuclei.

4. DNA extraction and HBV DNA nested PCR

Twenty patients who were negative for serological tests HBsAg were analyzed for the HBV DNA test. Total DNA was extracted from 15 snap frozen human sample using a Qiagen QIAamp DNA Mini Kit (Qiagen, Hilden, Germany), and 5 tissue slides using a ReliaPrep™ FFPE gDNA Miniprep System (Promega, Madison, WI, USA) according to the manufacture's instruction. For 15 snap frozen tissues, samples were lysed with 180uL of ALT buffer containing 20uL of protease K and incubated overnight in a 56℃ heat block. After the digestion, 200uL of AL buffer and 100% ethanol was added respectively. The solution was transferred to a spin column and centrifuged for 1 minute then washed with 500uL of AW1 and AW2 buffers. To elute the DNA, 200uL of AE buffer was added to the spin column and its concentration was quantified using a spectrophotometer NanoDrop (Thermo Scientific, Wilmington, DE). For tissue slides, 100% ethanol was added on the slide to collect the tissues in a tube and centrifuged for 5 minutes. Ethanol was removed and 200uL of lysis buffer was added with 10uL of Proteinase K and incubated overnight in a 56℃ heat block. After the digestion, 10uL of RNase A was added and incubated in a room temperature for 5 minutes. Then, 200uL of BL buffer, 240uL of 100% ethanol were added and transferred to the spin column and centrifuged for 30seconds at 13,000rpm. After washing, DNA was eluted using 30uL of distilled water. Using the DNA extracts from each sample, HBV DNA infection tests were performed by analyzing the presence of HBV genomes. Four different in-house nested-PCR amplification assays were followed to detect PreS-S, Precore–core, Pol and X HBV genomic regions. As previously described, we considered a case to be positive for HBV DNA when at least 2 different viral

genomic regions were detected[17]. The primer sets and PCR conditions are listed in Table2. PCR was performed with the AccuPower PCR Premix (Bioneer, Seoul, Korea) containing 10pM of primers, 250ng of genomic DNA and amplification protocol was as follows; 94℃ for 5 minutes, 40 cycles of 94℃ for 30 seconds, 30 seconds at each primer's annealing temperature and then 30 seconds at 72℃. The extension step was performed for 10 minutes at 72℃. A second round of PCR was performed for each sample and 1uL of the first round product was added to the mixture containing 10pM of second round primers and 18uL of distilled water. The second round of PCR was carried out using the same protocol described above. The final product and loading star (Dyne Bio, Seongnam, Korea) were loaded on a 2% agarose gel (MPBio, Santa Ana, CA, USA) and electrophoresis was performed. Out of 20 samples tested, 9 samples showed positivity for at least 2 of the different viral genomic regions.

Table 2. Sequences of the primers used for the HBV DNA nested PCR

Primer set	Sense primers	Antisense primers	T_a[2] (℃)
PreS-S	5′-GGTCACCATATTCTTGGGAA-3′	5′-AATGGCACTAGTAAACTGAG-3′	47.4
PreS-S[1]	5′-AATCCAGATTGGGACTTCAA-3′	5′-CCTTGATAGTCCAGAAGAAC-3′	47.4
Precore-core	5′-GCCTTAGAGTCTCCTGAGCA-3′	5′-GTCCAAGGAATACTAAC-3′	47.8
Precore-core[1]	5′-CCTCACCATACTGCACTCA-3′	5′-GAGGGAGTTCTTCTTCTAGG-3′	50.2
Pol	5′-CGTCGCAGAAGATCTCAATC-3′	5′-CCTGATGTGATGTTCTCCATG-3′	50.7
Pol[1]	5′-CCTTGGACTCATAAGGT-3′	5′-TTGAAGTCCCAATCTGGATT-3	45.7
X	5′-CCATACTGCGGAACTCCTAGC-3	5′-CGTTCACGGTGGTCTCCAT-3′	57.4
X[1]	5′-GCTAGGCTGTGCTGCCAACTG-3	5′-CGTAAAGAGAGGTGCGCCCCG-3′	59.7

[1]Applied in the second round.

[2]Annealing temperature.

5. Total RNA extraction, cDNA synthesis, and real-time quantitative reverse-transcriptase PCR

Total RNA was isolated from the snap frozen tissue samples (n = 38) using the Qiagen RNA isolation kit (Qiagen, Hilden, Germany) according to the manufacture's protocol. Briefly, 30mg snap frozen tissue sample were lysed with 600uL of RLT buffer containing 1% β-mercaptoethanol (Sigma Inc., St. Louis, MO, USA) and grinded with a homogenizer. After the disruption, equal volume of 70% ethanol was added and then transferred to a RNeasy spin column and centrifuged for 15 seconds. The column was washed with 700uL of RW1 buffer and 2 times with 500uL of RPE buffer. RNA was eluted using RNase-free water and purity was validated using gel electrophoresis and quantified with a spectrophotometer NanoDrop (Thermo Scientific, Wilmington, DE). First strand cDNA synthesis was performed using a TOPscript ^{tm} cDNA synthesis kit (Enzynomics, Daejeon, Korea) and 1ug of total RNA was mixed with 2× RT Buffer, 20× Enzyme Mix, and nuclease-free water. The mixtures were incubated for 60 minutes at 37℃, 5 minutes at 95℃ and then kept at 4℃. The Assay IDs of the primers were as follows: GAPDH (Hs_99999905_m1) and IL-6 (Hs_00985639_a1). Real-time quantitative RT-PCR was carried out using the Applied Biosystems 7500 Real-Time PCR System. The PCR master mix containing TaqMan 2× Universal PCR Master Mix, 20× TaqMan assay, and RT products in a 20μl reaction volume was processed as follows: 95℃ for 10 minutes, 40 cycles of 95℃ for 15 seconds and then 60℃ for 60 seconds. The signal was collected at the endpoint of every cycle. The mean values of the Ct, obtained in triplicate, were used for data analysis.

6. Statistical analyses

The data was analyzed using the SPSS version 17.0 software (SPSS Inc., Chicago, IL, USA) and presented as mean ± standard deviation. Differences between the 2 groups were analyzed using the Student's t-test, χ^2-test, Fisher's exact test. Univariable survival analyses were performed for overall and disease-free survivals using the Kaplan-Meier's method and log-rank tests. Statistical significance was reached when $P \leq 0.05$, and $P \leq 0.1$ was reported as a trend.

III. RESULTS

1. Pathological definition and selection of steatohepatitic HCC

HCCs with at least four of the following criteria were classified as steatohepatitic HCC: steatosis, tumor cell ballooning, Mallory-Denk bodies formation, pericellular fibrosis and inflammation. Twenty-one cases were selected as steatohepatitic HCCs according to the above criteria. For comparison, 34 conventional HCCs which did not fulfil the criteria of steatohepatitic HCC were selected. The histopathological characteristics of 21 steatohepatitic HCCs and 34 conventional HCCs are presented in Table 3 and Figure 1. Larger proportions of tumor cells with large droplet steatosis (P <0.001) were more frequently seen in steatohepatitic HCCs compared to conventional HCCs (*e.g.,* 52.3% *vs* 0%, based on lipid droplet level 'moderate' and 'severe', Fig 1A). Tumor cell ballooning (P <0.001) and Mallory-Denk bodies (P = 0.017) were also more frequently observed in steatohepatitic HCCs compared to conventional HCCs (*e.g.*, 61.9% *vs* 2.9% and 71.4% *vs* 38.2%, based on ballooning level 'marked' and Mallory-Denk Bodies 'presence', respectively, Fig

1B). Pericellular fibrosis was also a typical feature of steatohepatitic HCCs (*P* = 0.009, Fig 1C); marked pericellular fibrosis was more frequently seen in steatohepatitic HCCs (42.8%) compared to conventional HCCs (8.8%) and intratumoral inflammation was more frequently seen in steatohepatitic HCCs (*P* = 0.022, Fig 1D) compared to conventional HCCs (*e.g.,* 85.7% *vs* 55.9%, based on 'mild or moderate' presence in inflammation).

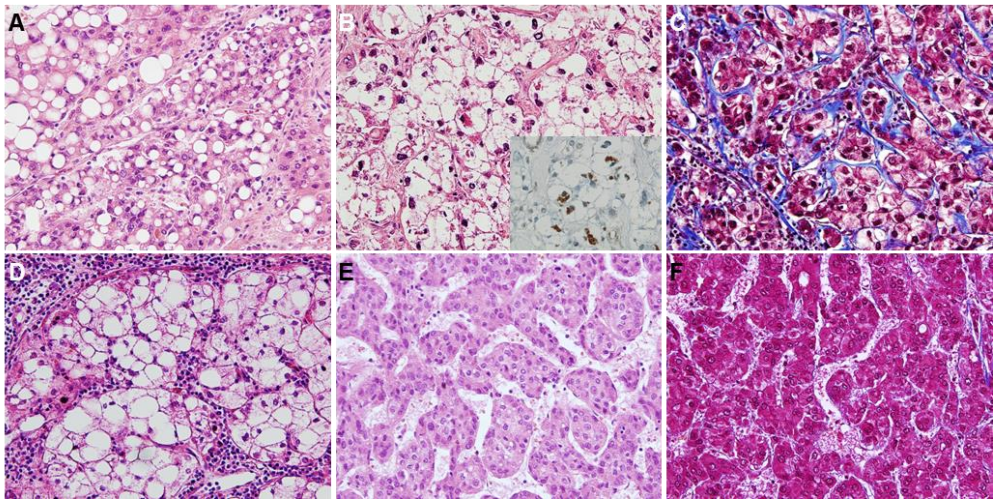

Figure 1. Histopathological features of steatohepatitic and conventional HCCs. Representative images demonstrating the pathological features of steatohepatitic HCC showing (**A**) large droplet steatosis, (**B**) ballooning change (inset: Mallory-Denk bodies, highlighted by ubiquitin stain), (**C**) pericellular fibrosis, (**D**) lymphocytic infiltration and (**E**, **F**) conventional HCC (x200) [(**A, B, D, E**) H&E, (**C**, **F**) Masson's trichrome, (**B,** inset) ubiquitin].

Table 3. A comparison of the histopathological features between steatohepatitic and conventional hepatocellular carcinomas

	SH-HCC (n=21)	C-HCC (n=34)	*P* value*
Large droplet steatosis (%)			**<0.001**
Absent or minimal	1 (4.8%)	21 (61.8%)	
Mild	9 (42.9%)	13 (38.2%)	
Moderate	7 (33.3%)	0 (0.0%)	
Severe	4 (19.0%)	0 (0.0%)	
Ballooning (%)			**<0.001**
None	0 (0.0%)	6 (17.6%)	
Focal	8 (38.1%)	27 (79.4%)	
Marked	13 (61.9%)	1 (2.9%)	
Mallory-Denk bodies (%)			**0.017**
Absent	6 (28.6%)	21 (61.8%)	
Present	15 (71.4%)	13 (38.2%)	
Pericellular fibrosis (%)			**0.009**
None	1 (4.8%)	5 (14.7%)	
Focal	11 (52.4%)	26 (76.5%)	
Marked	9 (42.8%)	3 (8.8%)	
Inflammation (%)			**0.022**
Minimal	3 (14.3%)	15 (44.1%)	
Mild or moderate	18 (85.7%)	19 (55.9%)	

Abbreviations: SH-HCC, steatohepatitic hepatocellular carcinoma; C-HCC, conventional hepatocellular carcinoma.
* Fisher's exact test and Pearson chi-square. Statistically significant *P* values are expressed in bold.

2. Other pathological characteristics of steatohepatitic HCC

We next compared the pathological parameters between steatohepatitic and conventional HCCs (Table 4). The steatohepatitic HCCs tended to be better differentiated compared to conventional HCCs, although statistical significance was not reached (major differentiation: $P = 0.096$, worst differentiation: $P = 0.086$). Other clinico-pathological parameters including tumor size, capsule formation, portal vein invasion, microvessel invasion, serosal invasion and satellite nodule showed no significant differences between two types of HCCs. In the adjacent non-tumor liver, NAFLD (including steatosis or steatohepatitis) was more frequently seen in steatohepatitic HCC cases compared to that of conventional HCCs (76.2% *vs* 35.2%).

Table 4. Pathological characteristics of steatohepatitic and conventional hepatocellular carcinomas

			SH-HCC (n=21)	C-HCC (n=34)	*P value**
Tumor	Tumor size (cm) [1]		3.3 ± 1.5	4.2 ± 3.5	0.308
	Capsule formation (%)	Complete	2 (9.5%)	9 (26.5%)	0.249
		Partial	11 (52.4%)	17 (50.0%)	
		None	8 (38.1%)	8 (23.5%)	
	Major differentiation (%)	Ⅰ	5 (23.8%)	2 (5.9%)	0.096
		Ⅱ	13 (61.9%)	24 (70.6%)	
		Ⅲ	3 (14.3%)	8 (23.5%)	
	Worst differentiation (%)	Ⅰ	2 (9.5%)	0 (0.0%)	0.086
		Ⅱ	11 (52.4%)	12 (35.3%)	
		Ⅲ	8 (38.1%)	21 (61.8%)	
		Ⅳ	0 (0.0%)	1 (2.9%)	
	Portal vein invasion (%)		1 (4.8%)	0 (0.0%)	0.382
	Microvessel invasion (%)		8 (38.1%)	15 (44.1%)	0.66
	Serosal invasion (%)		12 (57.1%)	18 (52.9%)	0.761
	Satellite nodule (%)		1 (4.8%)	4 (11.8%)	0.64
Non-tumor	NAFLD alone (%)		4 (19.1%)	2 (5.8%)	**0.010**
	NAFLD + B-viral chronic hepatitis (%)		12 (57.1%)	10 (29.4%)	
	B-viral chronic hepatitis alone (%)		3 (14.3%)	19 (55.9%)	
	Non-specific reactive hepatitis (%)		2 (9.5%)	3 (8.8%)	

Abbreviations: SH-HCC, steatohepatitic hepatocellular carcinoma; C-HCC, conventional hepatocellular carcinoma; NAFLD, non-alcoholic fatty liver disease.

* Fisher's exact test, Pearson chi-square and Student's t-test. Statistically significant *P* values are expressed in bold.

[1] Values expressed as mean ± standard deviation.

3. Clinical characteristics in steatohepatitic and conventional HCCs

In order to explore whether our cohort of steatohepatitic HCC is associated with metabolic syndrome risk factors, we next analyzed the clinical parameters of the steatohepatitic and conventional HCCs (Table 5). The patients with steatohepatitic HCC (n = 21) were significantly older compared to conventional HCC patients (n = 34) (66.7 ± 8.4 years *vs* 58.5 ± 10.1 years, mean ± SD, $P = 0.003$). There was no significant difference in gender distribution between the two types of HCCs ($P = 0.284$). Steatohepatitic HCC patients had higher BMI compared to that of conventional HCC patients (26.0 ± 4.6 kg/m^2 *vs* 23.7 ± 2.7 kg/m^2, mean ± SD, $P = 0.027$). The prevalent metabolic syndrome risk factors in steatohepatitic HCC patients, compared to those of conventional HCC patients, were central obesity (57.1% *vs* 32.4%, $P = 0.012$), diabetes (57.1% *vs* 29.4%, $P = 0.041$), and hypertriglyceridemia (23.8% *vs* 2.9%, $P = 0.028$). However, there were no significant differences in the prevalence of reduced high-density lipoprotein cholesterol (23.8% *vs* 14.7%, $P = 0.387$) and hypertension (47.6% *vs* 41.2%, $P = 0.640$) between the two groups. The prevalence of HBV infection and serum HBsAg and occult HBV infection did not differ among patients with steatohepatitic or those with conventional HCCs ($P = 0.300$, $P = 0.464$).Overall, steatohepatitic HCC patients more frequently demonstrated metabolic syndrome compared to conventional HCC patients (71.4% *vs* 41.2%, $P = 0.029$). Moreover metabolic syndrome with or without HBV infection did not differ between steatohepatitic and conventional HCCs ($P = 1.00$).

Table 5. Clinical characteristics of patients with steatohepatitic and conventional hepatocellular carcinomas

	SH-HCC (n=21)	C-HCC (n=34)	*P value**
Age (years) [1]	66.7 ± 8.4	58.5 ± 10.1	**0.003**
Sex (male:female)	8:13	18:16	0.284
Body mass index (kg/m^2) [1]	26.0 ± 4.6	23.7 ± 2.7	**0.027**
Central obesity (%) [2]	12 (57.1%)	11 (32.4%)	**0.012**
Low HDL cholesterol (%)[3]	5 (23.8%)	5 (14.7%)	0.387
Diabetes (%)[3]	12 (57.1%)	10 (29.4%)	**0.041**
Hypertension (%)[3]	10 (47.6%)	14 (41.2%)	0.64
Hypertriglyceridemia (%)[3]	5 (23.8%)	1 (2.9%)	**0.028**
HBV infection (%)	15 (71.4%)	29 (85.3%)	0.300
Serum HBsAg (+)	11 (52.4%)	24 (70.6%)	0.464
Occult HBV infection[4]	4 (19.1%)	5 (14.7%)	
Metabolic syndrome (%)[5]	15 (71.4%)	14 (41.2%)	**0.029**
MS (+)/HBV(-)	4 (19.0%)	3 (8.8%)	1.000
MS (+)/HBV(+)	11 (52.4%)	11 (32.4%)	

Abbreviations: SH-HCC, steatohepatitic hepatocellular carcinoma; C-HCC, conventional hepatocellular carcinoma; HDL, high-density lipoprotein; HBV, hepatitis B virus; hepatitis B virus surface antigen, HBsAg; MS, metabolic syndrome.

* Fisher's exact test, Pearson chi-square and Student's t-test. Statistically significant *P* values are expressed in bold.

[1] Values expressed as mean ± standard deviation.

[2] As defined by the International Diabetes Federation (IDF) ethnicity waist circumference criteria. Central obesity (waist circumference >90 cm in men and >80 cm in women).

[3] As defined by the US National Cholesterol Education Program Adult Treatment Panel III (NCEP ATP III) guidelines. Low HDL cholesterol (<40 mg/dL in men and <50 mg/dL in women), diabetes (elevated fasting plasma glucose levels ≥100 mg/dL or current use of anti-diabetic medication), hypertension (systolic blood pressure ≥130 mmHg or diastolic blood pressure ≥85 mmHg or current use of blood pressure medication) and hypertriglyceridemia (elevated serum triglycerides ≥150 mmHg or current use of antidyslipidemia medication).

[4] Occult HBV infection was considered positive when at least 2 different viral genomic regions (PreS-S, Precore–core, Pol and X HBV) were detected.

[5] The metabolic syndrome was defined by at least two of the five followings: central obesity, low HDL, diabetes, hypertension and hypertriglyceridemia.

4. Increased numbers of activated hepatic stellate cells in steatohepatitic HCC

The number of activated hepatic stellate cells was compared between steatohepatitic and conventional HCCs, by performing an immunohistochemical stain for α-SMA which is expressed in activated hepatic stellate cells (Fig. 2A, B). Interestingly, the number of activated hepatic stellate cells was higher in the tumor region of steatohepatitic HCCs compared to conventional HCCs (P = 0.049). In contrast, in the non-tumor region, the number of activated hepatic stellate cells showed no statistically significant difference between the two types of HCC (P = 0.358). In normal control livers, α-SMA positive stellate cells were rarely detected in the perisinusoidal spaces, and significantly lower than the non-neoplastic livers of both steatohepatitic and conventional HCCs (P = 0.001 for both).

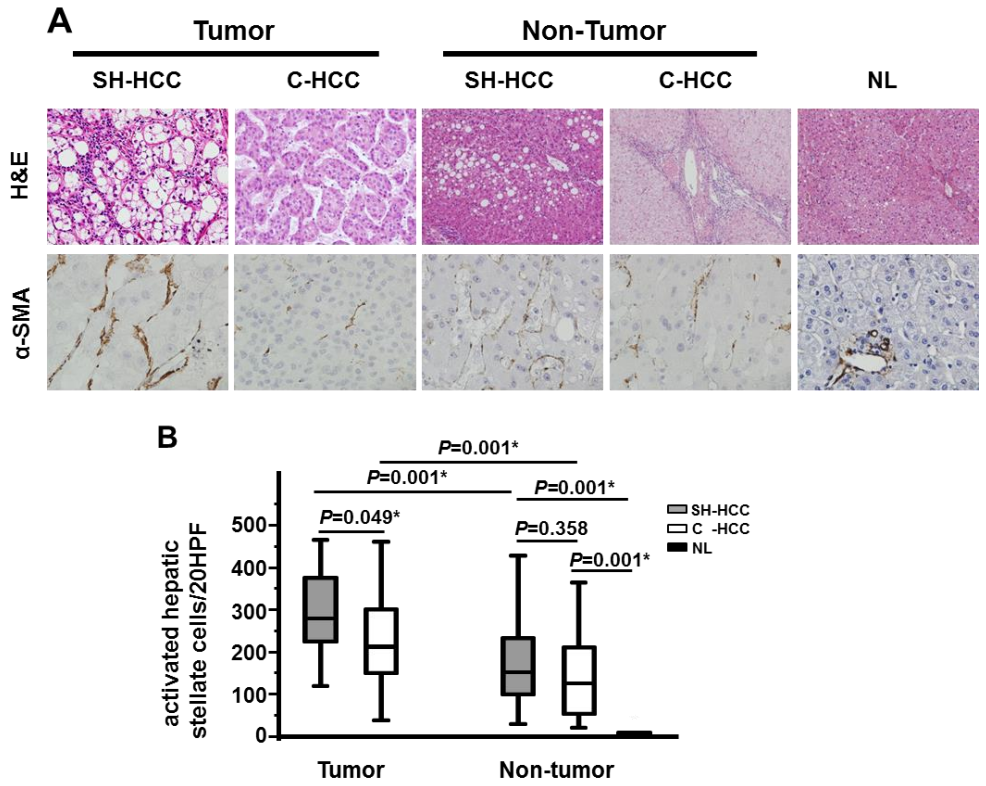

Figure 2. Activated hepatic stellate cells are increased in the tumor region of steatohepatitic HCC. (**A**) Representative H&E stain images of tumor and non-tumor regions of steatohepatitic HCC (SH-HCC) and conventional HCCs (C-HCC) and normal liver (NL) in the upper panels, and their representative immunohistochemical stains for α-SMA (brown) in the lower panels. [H&E, Original magnification, x200 (Tumor), x100 (Non-Tumor and NL); α-SMA, x400]. (**B**) The numbers of activated hepatic stellate cells were counted, using 20 randomly selected high power fields (x400) from the tumor and non-tumor regions of steatohepatitic and conventional HCCs, and compared to those from normal control liver. SH-HCC, steatohepatitic HCC; C-HCC, conventional HCC; NL, Normal control liver.

5. Increased numbers of activated hepatic stellate cells, expressing senescence-associated proteins and senescence-associated secretory phenotype (SASP) factor in the tumor region of steatohepatitic HCC

Our present finding that activated hepatic stellate cells were more frequently found in the tumor region of steatohepatitic HCC compared to conventional HCC prompted us to investigate whether a senescence-associated proteins and SASP of activated hepatic stellate cells is related to the development of steatohepatitic HCC. Activated hepatic stellate cells undergoing senescence generate DNA damage signals, in addition to the expression of cell cycle arrest markers such as $p21^{Waf1/Cip1}$. Therefore, we examined $p21^{Waf1/Cip1}$ and γ-H2AX, a DNA damage marker[13], in activated stellate cells, to explore whether senescence-associated protein expression is involved in steatohepatitic HCC. There was occasional co-expression of $p21^{Waf1/Cip1}$ and cytoplasmic α-SMA in stellate cells, and it was significantly higher in the tumor region of steatohepatitic HCCs compared to that of conventional HCCs (5.9% *vs* 4.2%, $P = 0.038$) (Fig. 3A). Next, we performed immunofluorescence staining of γ-H2AX (red fluorescence) and α-SMA (green fluorescence), in order to examine whether hepatic stellate cell activation in steatohepatitic HCCs is associated with DNA damage. Nuclear γ-H2AX was occasionally detected together with cytoplasmic α-SMA expression in the tumor region of steatohepatitic HCCs. The co-expression of γ-H2AX and α-SMA in the hepatic stellate cells was also higher in tumor region of steatohepatitic HCCs than conventional HCCs (27.3% *vs* 19.4%, $P = 0.066$) (Fig. 3B). To compare the proliferation activity of stellate cells between two types of HCC, a double-immunofluorescence staining was performed with Ki-67 (green fluorescence), a proliferation marker, and α-SMA (red fluorescence) (Fig. 3C). There were no significant differences in Ki-67/α-SMA co-

staining between the steatohepatitic and conventional HCCs (4.7% *vs* 4.1%, *P* = 0.775) (Fig. 3C). These findings indicate that activation of hepatic stellate cells accompanied with senescence-associated protein expression, including DNA damage and $p21^{Waf1/Cip1}$ are more involved in steatohepatitic HCCs compared to conventional HCCs.

As IL-6 is one of the major SASP factors in hepatic inflammation[13], which is one of key features of steatohepatitic HCC, we examined the correlation between hepatic stellate cell activation and IL-6 expression. Immunohistochemical staining showed IL-6 expression in tumor stromal region of steatohepatitic and conventional HCCs (Fig. 3D). When IL-6 staining area and intensity was semiquantitatively analyzed, we found that IL-6 was more highly expressed in the tumor region of steatohepatitic HCCs compared to conventional HCCs (*P* = 0.009) (Fig. 3D). Double immunofluorescence staining for IL-6 and α-SMA revealed that IL-6 (seen as red signals dispersed between stromal cell components) was either co-expressed in α-SMA-expressing cells or expressed alone without the green fluorescence (Fig. 3E). Specifically, IL-6/α-SMA co-expression was more frequently seen in the tumor regions of steatohepatitic HCCs than in conventional HCCs (29.3% *vs* 7.0%, *P* = 0.048) (Fig 3E). These findings indicate that SASP factor IL-6 expression occurs more frequently in steatohepatitic HCC. Collectively, steatohepatitic HCC expresses a SASP factor (IL-6) in the activated hepatic stellate cells, accompanied by the generation of senescent phenotype ($p21^{Waf1/Cip1}$ and γ-H2AX).

Furthermore, we examined the senescence-associated protein expressions in tumoral hepatocytes between the two types HCCs. However, there was no difference in $p21^{Waf1/Cip1}$, γ-H2AX-LI and Ki-67-LI expression between steatohepatitic and conventional HCCs in tumoral hepatocytes (*P* = 0.428, *P* = 0.283, *P* = 0.119,

respectively) (Fig. 4A~C). IL-6 mRNA levels, which were evaluated using whole tumor tissue were not different between the two groups (P = 0.486) (Fig. 4D).

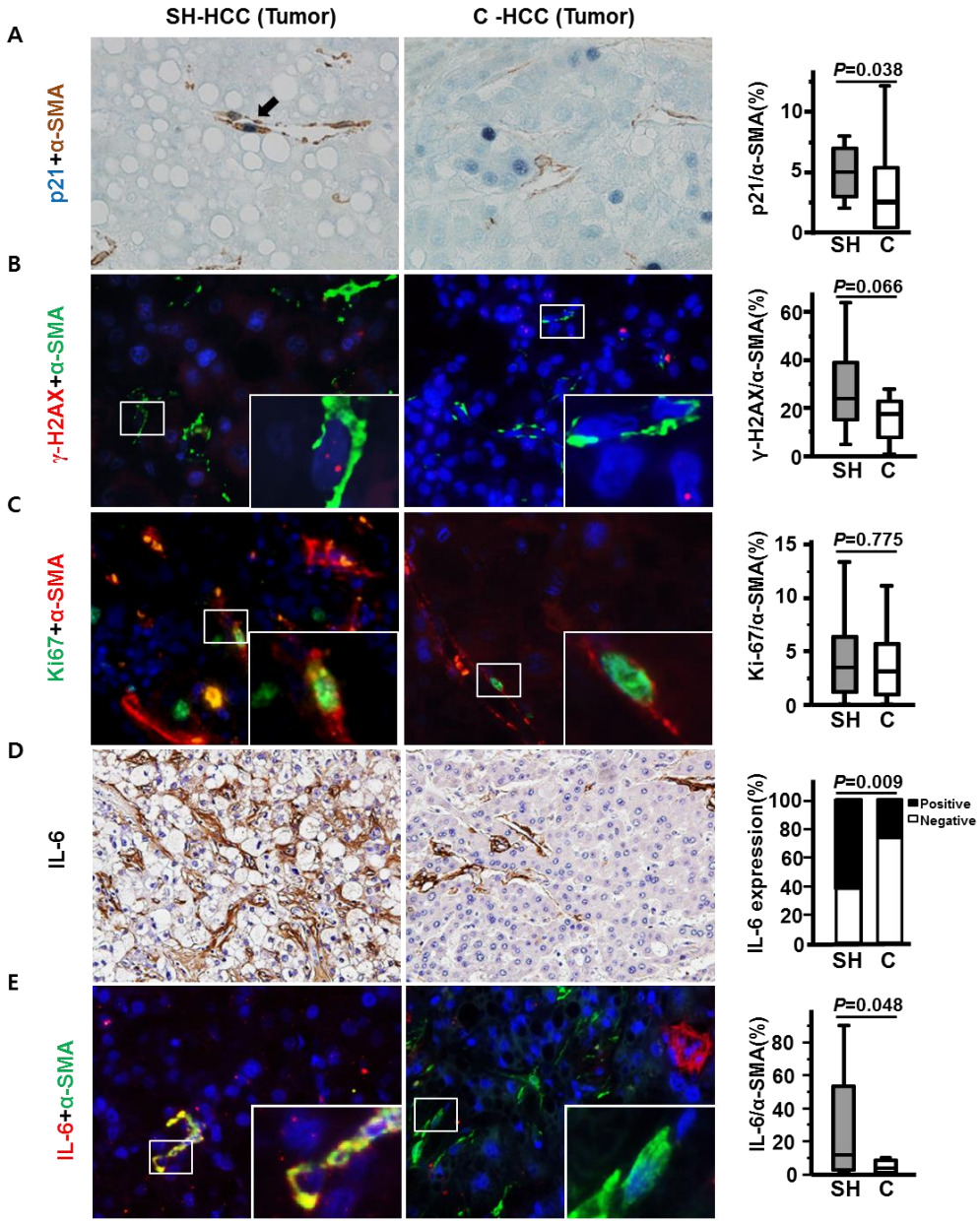

Figure 3. Increased numbers of activated hepatic stellate cells expressing senescence-associated proteins and senescence-associated secretory phenotype

(SASP) factor in the tumor region of steatohepatitic HCC. (**A**) Representative double immunohistochemistry images of the sections showing co-staining for $p21^{Waf1/Cip1}$ (blue) and α-SMA (brown) and box plot demonstrating the frequency of co-stained cells. Representative double immunofluorescence images and box plot demonstrating frequency of co-stained cells for (**B**) γ-H2AX (red fluorescence) and α-SMA (green fluorescence) (**C**) Ki-67 (green fluorescence) and α-SMA (red fluorescence) (**E**) IL-6 (red fluorescence) and α-SMA (green fluorescence) in tumor regions of the steatohepatitic HCC (SH-HCC) and conventional HCC (C-HCC). Nuclei were stained with DAPI. The merged fluorescence images of γ-H2AX/α-SMA, Ki67/α-SMA and IL-6/ α-SMA in the boxed areas are further magnified (inset). (original magnification x400). (**D**) Representative immunohistochemistry images for IL-6 (brown, original magnification x200) and protein expression level of IL-6 were compared in steatohepatitic and conventional HCCs. SH-HCC and SH, steatohepatitic HCC; C-HCC and C, conventional HCC.

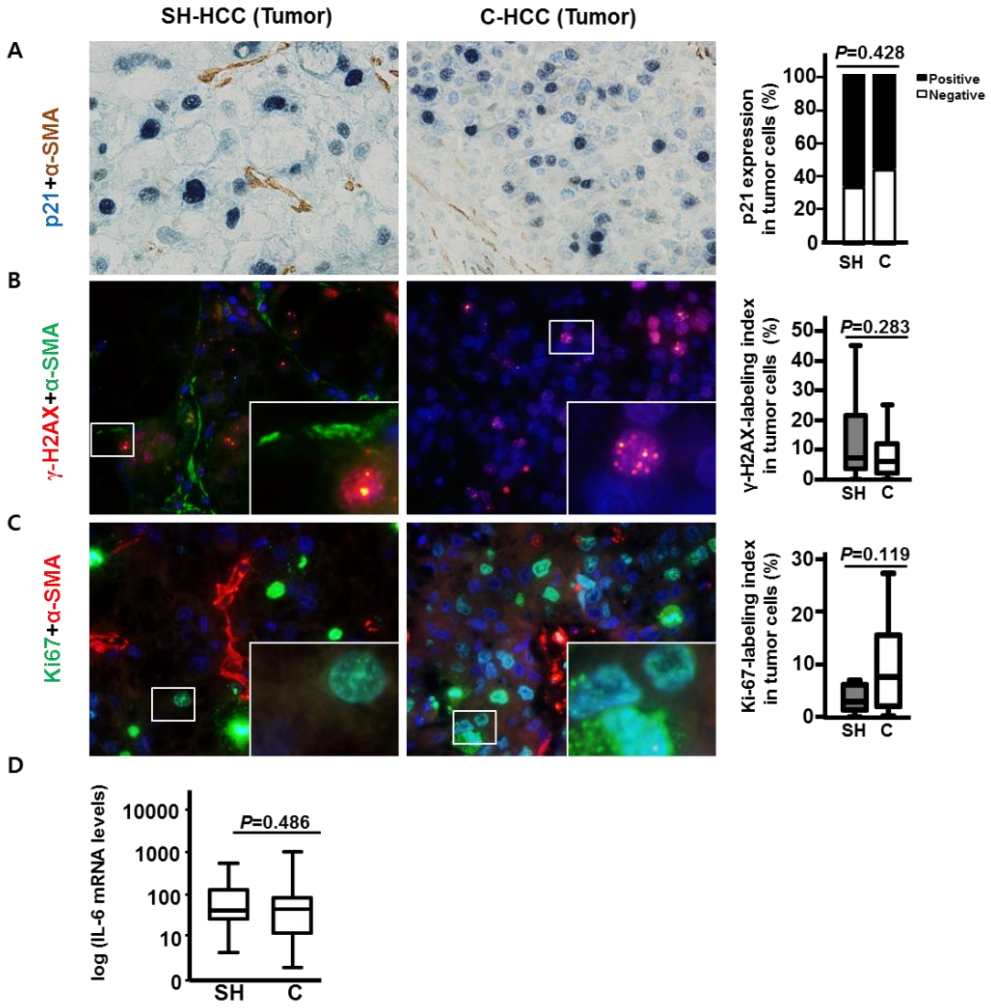

Figure 4. Senescence-associated proteins in the tumoral hepatocytes of steatohepatitic and conventional HCCs. (**A**) Representative double immunohistochemistry images of the sections showing $p21^{Waf1/Cip1}$ (blue) and α-SMA (brown) and protein expression of $p21^{Waf1/Cip1}$ in tumoral hepatocytes were compared. Representative immunofluorescence for (**B**) γ-H2AX (red fluorescence) and α-SMA (green fluorescence) and box plot demonstrating γ-H2AX-LI in tumoral hepatocytes and (**C**) Ki-67 (green fluorescence) and α-SMA (red fluorescence) and

box plot demonstrating Ki-67-LI in tumoral hepatocytes of steatohepatitic HCC (SH-HCC) and conventional HCC (C-HCC) were compared. Nuclei were stained with DAPI. The merged fluorescence images of γ-H2AX/α-SMA and Ki67/α-SMA in the boxed areas are further magnified (inset). (original magnification x400). (**D**) A comparison between the mRNA expression levels of IL-6 in the tumor region of steatohepatitic (n=14) and conventional HCCs (n=24). SH-HCC and SH, steatohepatitic HCC; C-HCC and C, conventional HCC.

6. Senescent-associated proteins and senescence-associated secretory phenotype (SASP) factor in activated hepatic stellate cells in the non-tumor region of steatohepatitic and conventional HCCs and normal control livers

We further compared the senescence-associated proteins ($p21^{Waf1/Cip1}$ and γ-H2AX) and SASP expression in the activated hepatic stellate cells and hepatocytes in the non-tumor region of steatohepatitic and conventional HCCs and normal control livers. As shown in Fig 5A, we found significant increase in the co-expression of nuclear $p21^{Waf1/Cip1}$ and cytoplasmic α-SMA in stellate cells in the non-tumor region of steatohepatitic HCCs compared to conventional HCCs (2.0% *vs* 0.73%, P = 0.019) (Fig 5A). Similarly to $p21^{Waf1/Cip1}$, the co-staining of γ-H2AX and α-SMA in the activated hepatic stellate cells was also higher in non-tumor regions of steatohepatitic HCCs than conventional HCCs (7.6% *vs* 3.8 %, P = 0.023) (Fig 5B). No differences were seen for Ki-67/α-SMA co-staining between the steatohepatitic and conventional HCCs in the non-tumor regions (0.8% *vs* 1.1 %, P = 0.389) (Fig 5C). The expression of IL-6 were more highly expressed in the non-tumor region of steatohepatitic HCC compared to that of conventional HCC; however, significance was not reached (P = 0.094) (Fig 5D). There was no difference in IL-6/α-SMA co-

expression in the non-tumor regions of these two types (5.9% *vs* 5.4%, $P = 0.299$) (Fig 5E). When the senescence-associated protein expression of $p21^{Waf1/Cip1}$, γ-H2AX-LI and Ki-67-LI was compared in the non-tumoral hepatocytes between steatohepatitic and conventional HCCs, there was no significant difference in their expression ($P = 0.208$, $P = 0.277$, $P = 0.927$, respectively) (Fig 6A~C).

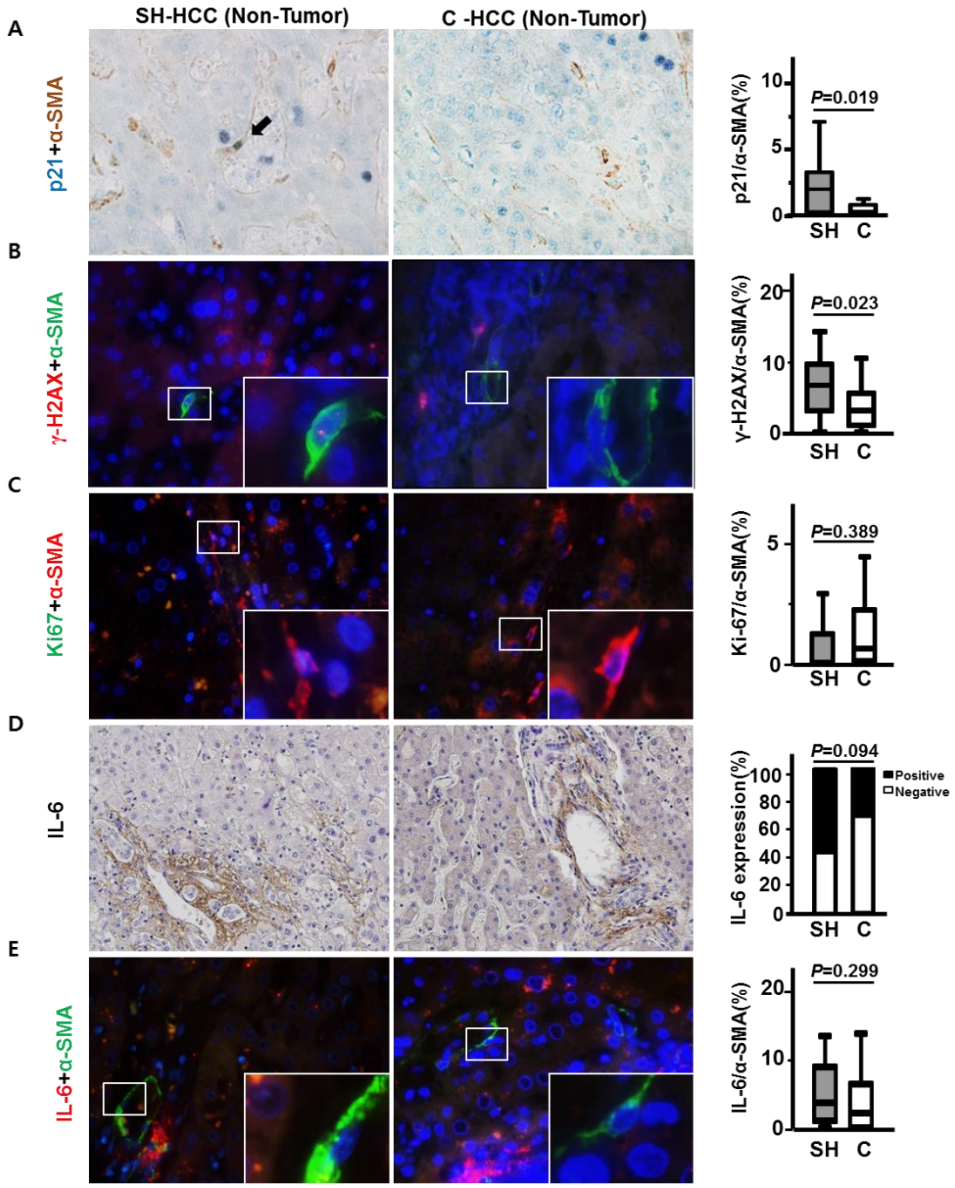

Figure 5. Senescence-associated proteins and senescence-associated secretory phenotype (SASP) factor in the activated hepatic stellate cells in the non-tumor region of steatohepatitic and conventional HCCs. Representative double immunohistochemistry images of the sections showing co-staining for $p21^{Waf1/Cip1}$ (blue) and α-SMA (brown) and box plot demonstrating the frequency of co-stained cells. Representative double immunofluorescence images and box plot demonstrating frequency of co-stained cells for (**B**) γ-H2AX (red fluorescence) and α-SMA (green fluorescence) (**C**) Ki-67 (green fluorescence) and α-SMA (red fluorescence) (**E**) IL-6 (red fluorescence) and α-SMA (green fluorescence) in non-tumor regions of the steatohepatitic HCC (SH-HCC) and conventional HCC (C-HCC). Nuclei were stained with DAPI. The merged fluorescence images of γ-H2AX/α-SMA, Ki67/α-SMA and IL-6/ α-SMA in the boxed areas are further magnified (inset). (original magnification x400). (**D**) Representative immunohistochemistry images for IL-6 (brown, original magnification x200) and protein expression level of IL-6 were compared in the non-tumor regions of steatohepatitic and conventional HCCs. SH-HCC and SH, steatohepatitic HCC; C-HCC and C, conventional HCC.

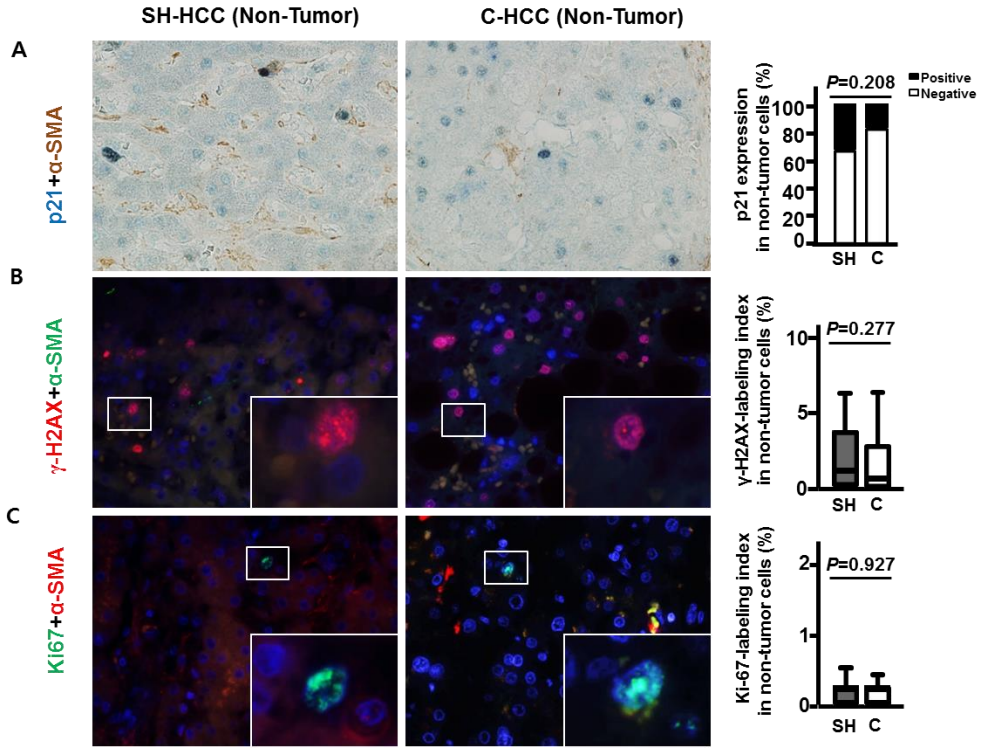

Figure 6. Senescence-associated proteins in the non-tumoral hepatocytes of steatohepatitic and conventional HCCs. (**A**) Representative double immunohistochemistry images of the sections showing $p21^{Waf1/Cip1}$ (blue) and α-SMA (brown) and protein expression of $p21^{Waf1/Cip1}$ in non-tumoral hepatocytes were compared. Representative immunofluorescence for (**B**) γ-H2AX (red fluorescence) and α-SMA (green fluorescence) and box plot demonstrating γ-H2AX-LI in non-tumoral hepatocytes and (**C**) Ki-67 (green fluorescence) and α-SMA (red fluorescence) and box plot demonstrating Ki-67-LI in non-tumoral hepatocytes of steatohepatitic HCC (SH-HCC) and conventional HCC (C-HCC) were compared. Nuclei were stained with DAPI. The merged fluorescence images of γ-H2AX/α-SMA and Ki67/α-SMA in the boxed areas are further magnified (inset). (original magnification x400). SH-HCC and SH, steatohepatitic HCC; C-

HCC and C, conventional HCC.

In normal control livers (n=5), only one case showed co-staining of $p21^{Waf1/Cip1}$, γ-H2AX in the activated hepatic stellate cells and Ki-67, IL-6 were not detected. (Fig. 7A~F).

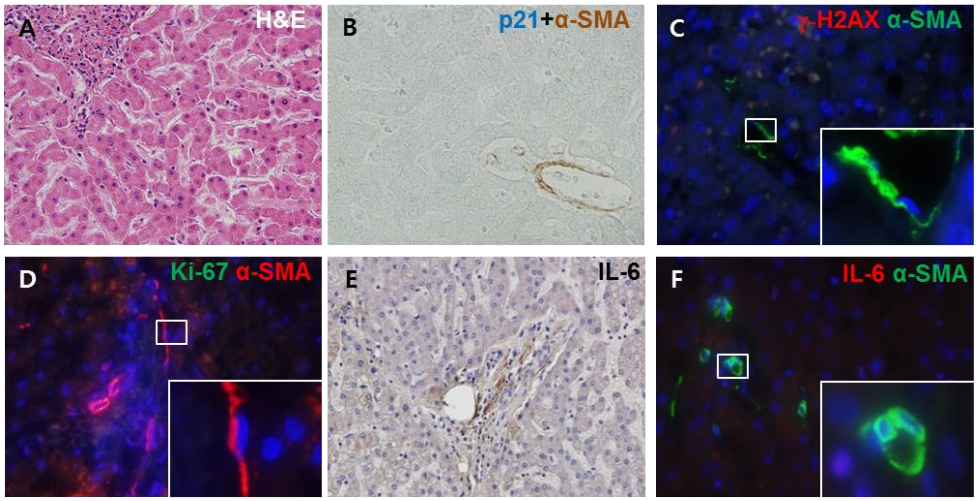

Figure 7. Senescence-associated proteins and senescence-associated secretory protein (SASP) factor in the normal control liver. (**A**) Representative H&E and (**B**) double immunohistochemistry image of the sections showing $p21^{Waf1/Cip1}$ (blue) and α-SMA (brown). (**C**) Representative double immunofluorescence images of the sections positive for γ-H2AX (red fluorescence) and α-SMA (green fluorescence), (**D**) Ki-67 (green fluorescence) and α-SMA (red fluorescence) and (**F**) IL-6 (red fluorescence) and α-SMA (green fluorescence) in normal control liver. Nuclei were stained with DAPI. The merged fluorescence images of γ-H2AX/α-SMA, Ki67/α-SMA and IL-6/ α-SMA in the boxed areas are further magnified (inset). (original magnification x400). (**E**) Representative immunohistochemistry images for IL-6 (brown, original magnification x200).

7. Survival analysis in steatohepatitic and conventional HCCs

To explore the prognostic significance of steatohepatitic HCCs, we analyzed patient survival after surgical resection. One patient from conventional HCC who had liver transplantation was excluded from the survival analysis. The median follow-up time after surgical resection was 30.5 months (range, 1~73). Kaplan-Meier plots revealed no significant difference in both disease-free (P = 0.602) and overall survivals (P = 0.709) between steatohepatitic (n = 21) and conventional HCCs (n = 33) (Fig. 8 A, B).

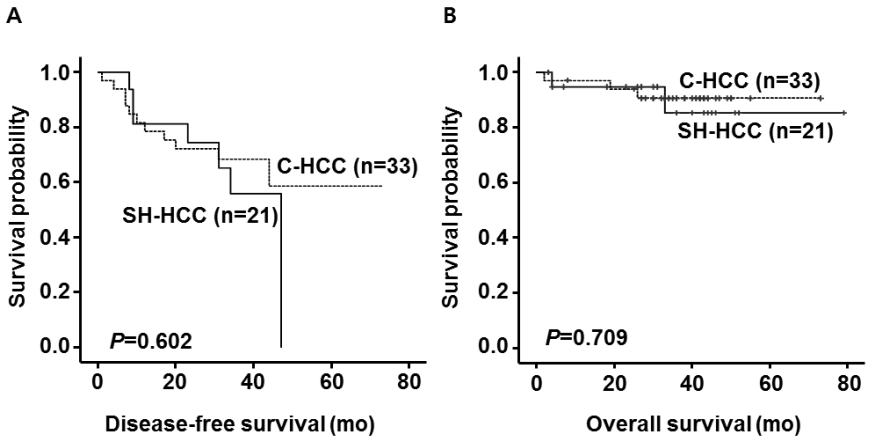

Figure 8. Survival analysis results. Kaplan–Meier's plot analysis for (**A**) disease-free and (**B**) overall survival in steatohepatitic HCC (SH-HCC) and conventional HCC (C-HCC). SH-HCC, steatohepatitic HCC; C-HCC, conventional HCC.

IV. DISCUSSION

The steatohepatitic variant of HCC has been reported to be more frequently associated with metabolic syndrome and NAFLD compared to conventional HCCs[7-9]. Due to changes in lifestyle and diet, metabolic syndrome is increasing in Asia

including Korea as well as Western countries, and in the near future it is expected to exceed viral hepatitis as an etiology of chronic liver disease[18]. Most studies with steatohepatitic HCC have mainly dealt with HCV, and its relation with HBV or molecular pathogenesis remains unclear. In this study we focused on HCC patients with non-C viral, non-alcoholic and non-autoimmune hepatitis etiologies, and performed HBV DNA test to more specifically understand the association between steatohepatitic HCC with HBV and metabolic syndrome.

In this study, steatohepatitic HCCs showed older age, increased metabolic syndrome risk factors, better differentiation of tumor and more prevalent NAFLD in non-tumor regions compared to conventional HCCs, and it was consistent with previous reports[7-9]. Interestingly, we found that prevalence of HBV infection did not differ between the two types of HCCs. In addition, most of the steatohepatitic HCCs demonstrated NAFLD with HBV in the non-tumor regions. Of note, previous studies in *in vitro* and transgenic mice have shown that HBV genome, hepatitis B virus protein X (HBx), can up-regulate lipogenic genes and promote steatosis[19, 20]. Furthermore, HBx transgenic mice fed a high fat diet stabilizes HBx protein using fatty acid and promotes steatohepatitis[21]. HBV infection has also been shown to alter bile acid and cholesterol metabolism[22]. Further studies are needed to understand the complex interplay between HBV infection and its effect on metabolic syndrome and neoplastic hepatocytes.

In normal liver, hepatic stellate cells are mostly quiescent retinoid-storing cells. Upon liver injury, hepatic stellate cells become activated to become highly fibrogenic cells and secrete various cytokines and interact with hepatocytes and the microenvironment[23]. Recent research showed that dietary or genetically induced-obese mice had changes in the microbiome and its metabolite promoted SASP in

hepatic stellate cells that led to HCC development.[13] When cells undergo senescence, they develop inflammatory cytokines, chemokines and proteases also known as SASP[24]. Some SASP factors, such as IL-6 are known to be associated with NAFLD and obesity-associated cancer[25, 26]. In the present study, we demonstrated increased activated hepatic stellate cells in tumor region of steatohepatitic HCCs compared to conventional HCC. In addition, activated hepatic stellate cells showed increased expression of cellular senescence marker such as p21 $^{Waf1/Cip1}$ and DNA damage marker γ-H2AX in steatohepatitic HCCs both in tumor and non-tumor regions compared to conventional HCC. To examine if this response further correlated with SASP factor, we performed IL-6 immunohistochemistry and found increased expression of IL-6 in the steatohepatitic HCCs. To see whether activated hepatic stellate cells secrete IL-6, we performed double immunofluorescence and found that these stellate cells also secrete IL-6 and this was more prominent in steatohepatitic HCCs compared to conventional HCCs. Unlike in the tumor, we did not see differences in the number of activated hepatic stellate cells and IL-6/α-SMA co-expressing cells in the non-tumor regions between two types of HCCs. Therefore, it is suggested that activated hepatic stellate cells showing features of SASP could play important roles in the pathogenesis of steatohepatitic HCC.

There are several limitations to our study. The current study was retrospective in design and some of the metabolic syndrome related data were missing. In addition, even though we found increased IL-6 expression in steatohepatitic HCCs, there were no significant differences in the clinicopathological factors related to tumor aggressiveness or survival between steatohepatitic and conventional HCCs unlike the previous report by Shibahara et al[9]. Prospective studies based on large number

of cases are needed to further understand the interplay between SASP factor and its effect on the biological behavior of steatohepatitic HCC.

V. CONCLUSION

Steatohepatitic HCC showed higher incidence of metabolic syndrome with or without HBV than conventional HCC, and non-tumoral liver of steatohepatitic HCC also showed higher incidence of NAFLD compared to that of conventional HCC. Activated hepatic stellate cells expressing $p21^{Waf1/Cif1}$, γ-H2AX and IL-6 were more frequently found in tumoral region of steatohepatitic HCC compared to conventional HCC. Non-tumoral liver of steatohepatitic HCC also showed higher number of activated stellate cells expressing γ-H2AX and $p21^{Waf1/Cif1}$ compared to that of conventional HCC. Therefore, steatohepatitic HCC is suggested as a distinctive variant of HCC, which is closely associated with metabolic syndrome with or without chronic B viral hepatitis. Activated hepatic stellate cells with SASP signature is considered to be important in the pathogenesis of steatohepatitic HCC.

REFERENCES

1. Angulo P, Lindor KD. Non-alcoholic fatty liver disease. Journal of gastroenterology and hepatology 2002;17 Suppl:S186-90.

2. Neuschwander-Tetri BA, Caldwell SH. Nonalcoholic steatohepatitis: summary of an AASLD Single Topic Conference. Hepatology 2003;37(5):1202-19.

3. Eckel RH, Grundy SM, Zimmet PZ. The metabolic syndrome. Lancet 2005;365(9468):1415-28.

4. Marchesini G, Bugianesi E, Forlani G, Cerrelli F, Lenzi M, Manini R, et al. Nonalcoholic fatty liver, steatohepatitis, and the metabolic syndrome. Hepatology 2003;37(4):917-23.

5. Lim S, Shin H, Song JH, Kwak SH, Kang SM, Yoon JW, et al. Increasing Prevalence of Metabolic Syndrome in Korea The Korean National Health and Nutrition Examination Survey for 1998-2007. Diabetes Care 2011;34(6):1323-8.

6. Chen CL, Yang HI, Yang WS, Liu CJ, Chen PJ, You SL, et al. Metabolic factors and risk of hepatocellular carcinoma by chronic hepatitis B/C infection: a follow-up study in Taiwan. Gastroenterology 2008;135(1):111-21.

7. Salomao M, Yu WM, Brown RS, Jr., Emond JC, Lefkowitch JH. Steatohepatitic hepatocellular carcinoma (SH-HCC): a distinctive histological variant of HCC in hepatitis C virus-related cirrhosis with associated NAFLD/NASH. The American journal of surgical pathology 2010;34(11):1630-6.

8. Salomao M, Remotti H, Vaughan R, Siegel AB, Lefkowitch JH, Moreira RK. The steatohepatitic variant of hepatocellular carcinoma and its association with underlying steatohepatitis. Human pathology 2012;43(5):737-46.

9. Shibahara J, Ando S, Sakamoto Y, Kokudo N, Fukayama M. Hepatocellular carcinoma with steatohepatitic features: a clinicopathological study of Japanese

patients. Histopathology 2014;64(7):951-62.

10. Merican I, Guan R, Amarapuka D, Alexander MJ, Chutaputti A, Chien RN, et al. Chronic hepatitis B virus infection in Asian countries. Journal of gastroenterology and hepatology 2000;15(12):1356-61.

11. Friedman SL. Hepatic stellate cells: protean, multifunctional, and enigmatic cells of the liver. Physiological reviews 2008;88(1):125-72.

12. Mederacke I, Hsu CC, Troeger JS, Huebener P, Mu X, Dapito DH, et al. Fate tracing reveals hepatic stellate cells as dominant contributors to liver fibrosis independent of its aetiology. Nature communications 2013;4:2823.

13. Yoshimoto S, Loo TM, Atarashi K, Kanda H, Sato S, Oyadomari S, et al. Obesity-induced gut microbial metabolite promotes liver cancer through senescence secretome. Nature 2013;499(7456):97-101.

14. Kleiner DE, Brunt EM, Van Natta M, Behling C, Contos MJ, Cummings OW, et al. Design and validation of a histological scoring system for nonalcoholic fatty liver disease. Hepatology 2005;41(6):1313-21.

15. Expert Panel on Detection E, Treatment of High Blood Cholesterol in A. Executive Summary of The Third Report of The National Cholesterol Education Program (NCEP) Expert Panel on Detection, Evaluation, And Treatment of High Blood Cholesterol In Adults (Adult Treatment Panel III). Jama 2001;285(19):2486-97.

16. Alberti KG, Zimmet P, Shaw J. Metabolic syndrome--a new world-wide definition. A Consensus Statement from the International Diabetes Federation. Diabetic medicine : a journal of the British Diabetic Association 2006;23(5):469-80.

17. Pollicino T, Squadrito G, Cerenzia G, Cacciola I, Raffa G, Craxi A, et al. Hepatitis B virus maintains its pro-oncogenic properties in the case of occult HBV

infection. Gastroenterology 2004;126(1):102-10.

18. Loomba R, Sanyal AJ. The global NAFLD epidemic. Nature reviews Gastroenterology & hepatology 2013;10(11):686-90.

19. Kim KH, Shin HJ, Kim K, Choi HM, Rhee SH, Moon HB, et al. Hepatitis B virus X protein induces hepatic steatosis via transcriptional activation of SREBP1 and PPARgamma. Gastroenterology 2007;132(5):1955-67.

20. Na TY, Shin YK, Roh KJ, Kang SA, Hong I, Oh SJ, et al. Liver X receptor mediates hepatitis B virus X protein-induced lipogenesis in hepatitis B virus-associated hepatocellular carcinoma. Hepatology 2009;49(4):1122-31.

21. Cho HK, Kim SY, Yoo SK, Choi YH, Cheong J. Fatty acids increase hepatitis B virus X protein stabilization and HBx-induced inflammatory gene expression. The FEBS journal 2014;281(9):2228-39.

22. Oehler N, Volz T, Bhadra OD, Kah J, Allweiss L, Giersch K, et al. Binding of hepatitis B virus to its cellular receptor alters the expression profile of genes of bile acid metabolism. Hepatology 2014;60(5):1483-93.

23. Yin C, Evason KJ, Asahina K, Stainier DY. Hepatic stellate cells in liver development, regeneration, and cancer. The Journal of clinical investigation 2013;123(5):1902-10.

24. Coppe JP, Desprez PY, Krtolica A, Campisi J. The senescence-associated secretory phenotype: the dark side of tumor suppression. Annual review of pathology 2010;5:99-118.

25. Park EJ, Lee JH, Yu GY, He G, Ali SR, Holzer RG, et al. Dietary and genetic obesity promote liver inflammation and tumorigenesis by enhancing IL-6 and TNF expression. Cell 2010;140(2):197-208.

26. Wieckowska A, Papouchado BG, Li Z, Lopez R, Zein NN, Feldstein AE.

Increased hepatic and circulating interleukin-6 levels in human nonalcoholic steatohepatitis. The American journal of gastroenterology 2008;103(6):1372-9.

< ABSTRACT (IN KOREAN)>

지방간염성 간암에서 활성화된 간 성상세포의
노화활성인자 발현

<지도교수 박 영 년>

연세대학교 대학원 의과학과

이 지 산

최근 종양 내에 지방간염의 병리학적 소견을 보이는 간암인 지방간염성 간암 (steatohepatitic HCC)이 대사증후군과 함께 비알코올성 지방간염을 동반한 C형 간염 간암환자에서 보고되었다. 한국을 비롯한 동양에서 최근 대사증후군의 발생이 급격히 증가하고 있으며, 또한 만성 B형간염의 발생빈도가 높은 실정이나, 대사증후군을 동반한 만성 B형 간염 환자에서의 지방간염성 간암의 발생 및 분자병리학적 특징은 아직 밝혀지지 않았다. 본 연구에서는 C형 간염, 알코올성 간염, 그리고 자가면역성 간염을 제외한 간암환자에서 지방간염성 간암 (SH-HCC) 21명과 전형적인 간세포암종의 병리학적 소견을 보이는 간암 환자군 (C-HCC) 34명을 선별하여 분자병리학적 특성을 비교하였다. B형 간염의 유무는 혈청 HBsAg 검사 및 간조직에서의 HBV DNA에 대한 이중 중합효소 연쇄반응으로 검색하였으며, 특히 활성화된 간 성상세포에서의 노화활성인자 발현에 중점을 두어 분자병리학적 특성을 비교하였다. 이중 면역염색 및 면역형광 염색방법을 이용하여 α-smooth muscle actin (α-SMA), $p21^{Waf1/Cip1}$, γ-H2AX 그리고 IL-6에 대한 발현을 비교하였다. SH-HCC

군에서 C-HCC군에 비해 발생연령이 높았으며, BMI, 당뇨, 복부비만, 고지혈증 및 비알코올성 지방간의 발생빈도가 더 높았다 (P <0.05). SH-HCC군에서 C-HCC군에 비하여 대사증후군의 발생이 높았으며 (P = 0.029), 반면 만성 B형간염 발생은 두 군간의 차이를 보이지 않았다. SH-HCC의 종양내에서 활성화된 간성상세포가 C-HCC에 비하여 더 자주 관찰되었으며, 활성 간성상세포에서 발현하는 $p21^{Waf1/Cip1}$, IL-6 (P <0.05) 및 γ-H2AX (P = 0.066)의 발현정도도 SH-HCC에서 의 C-HCC에 비하여 높았다. 간의 비종양 부위에서도 $p21^{Waf1/Cip1}$, γ-H2AX 를 발현하는 활성화된 간 성상세포가 SH-HCC에서 C-HCC의 비 종양 부분에 비해 더 많았다(P <0.05). 활성화된 간 성상세포에서의 Ki-67 발현은 종양, 비 종양 부분에서 두 군간에 차이가 없었다.

이상의 소견으로 SH-HCC은 대사증후군과 연관된 HCC의 특징적인유형으로 생각되며, B형간염 환자에서도 대사증후군이 동반될 경우 SH-HCC이 발생이 증가된다. 또한 SH-HCC 간암발생에 활성화된 간 성상세포에서에서 발현하는 노화인자 ($p21^{Waf1/Cif1}$, γ-H2AX) 및 노화활성인자 (IL-6)가 중요한 역할을 할 것으로 생각한다.

핵심되는 말: 간암, 지방간염성 간암, 비알코올성 지방간질환, 대사증후군, 간성상세포 활성, 노화세포의 분비활성